Icelandic Low and Azores High Migrations Impact Florida Current Transport in Winter

SULTAN HAMEED,[a] CHRISTOPHER L. P. WOLFE,[a] AND LEQUAN CHI[b]

[a] *School of Marine and Atmospheric Sciences, Stony Brook University, State University of New York, Stony Brook, New York*
[b] *Skidaway Institute of Oceanography, The University of Georgia, Savannah, Georgia*

(Manuscript received 20 May 2020, in final form 8 July 2021)

ABSTRACT: Previous work by Meinen and coworkers to find an association between variations of annually averaged Florida Current transport (FCT) and the North Atlantic Oscillation (NAO) has yielded negative results. Here we show that the Florida Current in winter is impacted by displacements in the positions of the Azores high and the Icelandic low, the constituent pressure centers of the NAO. As a one-dimensional representation of North Atlantic atmospheric circulation, the NAO index does not distinguish displacements of the pressure centers from fluctuations in their intensity. FCT is significantly correlated with Icelandic low longitude with a lag of less than one season. We carried out perturbation experiments in the ECCOv4 model to investigate these correlations. These experiments reveal that east–west shifts of the Icelandic low perturb the wind stress in midlatitudes adjacent to the American coast, driving downwelling (through longshore winds) and offshore sea level anomalies (through wind stress curl) that travel to the Straits of Florida within the same season. FCT is also correlated with the latitude variations of both the Icelandic low and the Azores high with a lag of 4 years. Regression analysis shows that latitude variations of the Icelandic low and the Azores high are associated with positive wind stress curl anomalies over extended regions in the ocean east of Florida. Rossby wave propagation from this region to the Straits of Florida has been suggested as a mechanism for perturbing FCT in several previous studies by various researchers, as detailed in sections 4b and 5.

KEYWORDS: Atmosphere-ocean interaction; Boundary currents

1. Introduction

The Florida Current is the ''headwaters'' of the Gulf Stream and a component of the northward surface branch of the Atlantic meridional overturning circulation (AMOC). Baringer and Larsen (2001) analyzed annually averaged Florida Current transport (FCT) during 1982–98 and found a significant correlation with the North Atlantic Oscillation (NAO) after the two data series were smoothed by a 2-yr running average. Meinen et al. (2010) reviewed available records of FCT measurements and analyzed the current's variations on different time scales during 1964–2007. They found that the correlation between the NAO and FCT reported by Baringer and Larsen (2001) for 1982–98 does not extend outside that time window.

The purpose of this paper is to report that the impact of the NAO on FCT emerges when we decompose the NAO into its two constituent centers of action, the Icelandic low (IL) and the Azores high (AH). These centers vary not only in pressure but also in position.

A traditional definition of the NAO index is the difference in atmospheric pressure anomalies at the Azores Island or Lisbon, Portugal, to represent the AH, and at Reykjavik, Iceland, to represent the IL (Hurrell 1995). Another definition of the NAO index is based on empirical orthogonal function (EOF) analysis of sea level pressure or geopotential heights over the North Atlantic Ocean. The first EOF pattern contains the largest variance, and its principal component (PC) is designated as the NAO index (Barnston and Livezey 1987; Hurrell et al. 2003). In both these definitions the positions of the AH and the IL are effectively fixed. This is a limiting assumption because the IL and the AH are known to migrate considerably and change shape from month to month. The distribution of wind stress over the ocean changes as the IL and AH change in position or intensity. Therefore, additional useful information about the atmosphere's impact on ocean circulation can be obtained by considering variations in the location as well as the intensity of the AH and IL. For example, Hameed and Piontkovski (2004) found that correlations between the meridional movement of the Gulf Stream North Wall and IL pressure and longitude are significantly greater than with the NAO. Moreover, the correlations with the IL lead to the conclusion that the North Wall shifts are regulated more effectively by southward flow of the Labrador Current, as suggested by Rossby and Benway (2000), and less by Rossby waves generated by modulation of zonal winds by the NAO. Sanchez-Franks et al. (2016) showed that the position of the North Wall can be successfully predicted one year in advance by including IL pressure and longitude among the predictors. Bakalian et al. (2007) found that the IL latitude impacts the frequency of Greenland tip jet events that can trigger downwelling in the Irminger Sea.

Possible mechanisms that can affect FCT have been investigated in several studies. Anderson and Corry (1985a) described results from a two-layer model extending from 10°S to 50°N in the Atlantic, correctly reproducing the seasonal cycle of transport through the Straits of Florida. Their model

Supplemental information related to this paper is available at the Journals Online website: https://doi.org/10.1175/JPO-D-20-0108.s1.

Corresponding author: Sultan Hameed, sultan.hameed@stonybrook.edu

DOI: 10.1175/JPO-D-20-0108.1

suggested that seasonal variations in FCT transport are related to topographically modified barotropic Rossby waves generated by curl of the wind stress divided by the depth of the water column (i.e., curl $\boldsymbol{\tau}/H$). In addition, baroclinic Kelvin waves from the north induce transport variations. In another paper, Anderson and Corry (1985b) conducted numerical experiments in which wind forcing was restricted to particular regions and found that the Caribbean Sea and western Atlantic north of the Straits of Florida make important contributions to Florida Current.

Greatbatch and Goulding (1989) used a barotropic model extending from 10°S to 80°N and driven by monthly mean wind stresses to calculate the seasonal variation of the volume transport streamfunction over the North Atlantic. Their model showed enhanced circulation in the subpolar and subtropical gyres in January and February. The model showed significant streamfunction anomalies along the Atlantic coast of North America that extended south to Florida.

DiNezio et al. (2009) analyzed the relationship between the variability of NAO and Atlantic wind stress curl in the 3–12-yr frequency band during 1982–2007 in a latitude band centered on 27°N. They found that the correlation between the NAO and wind stress curl was statistically significant only at the 67% level. Based on this correlation, they suggested that the anticorrelation between the NAO and FCT was due to the propagation of first mode baroclinic Rossby waves forced by NAO-induced wind stress curl variations in the ocean interior.

Czeschel et al. (2012) used the Massachusetts Institute of Technology general circulation model (MITgcm; Marshall et al. 1997) and its adjoint to identify regions where the wind stress influences the annual cycle of FCT transport and estimate the associated time lags. The adjoint study showed a large contribution to FCT variations from barotropic waves trapped near the coast and generated by wind stress anomalies along the shelf north of Straits of Florida, with sensitivities extending as far north as the Labrador Sea. The model suggested that alongshore wind stress anomalies perturb coastal upwelling and fast barotropic waves carry these signals southward, reaching Straits of Florida within one month. In addition, there was a significant contribution from long baroclinic planetary Rossby waves generated by wind stress curl forcing in the interior ocean and by interactions between currents and topography east of the Grand Banks of Newfoundland. Their model suggested that the annual cycle of FCT transport is driven by wind forcing and that thermohaline forcing does not play a significant role.

Domingues et al. (2019) used a high-resolution (1/25°) numerical model of the subtropical west Atlantic to study eddy migration from the open ocean into the Straits of Florida. They showed that eddy-induced perturbations generated east of the Bahamas travel through the Northwest Providence Channel to reach the Straits of Florida, but that the Antilles Current acts as a barrier to baroclinic signals originating in the open ocean. In addition, generation of coastally trapped waves by interaction of eddies with the Gulf Stream near Cape Hatteras was found to be an important source of perturbations to the FCT.

There is also evidence that FCT variability is related to transport fluctuations upstream in the Yucatan Channel. Lin et al. (2009) reported that current transport over an 11-month period in the Yucatan channel is correlated with Florida Current variations. Using an eddy-permitting model, they found that a large part of the interannual to decadal fluctuations in Florida Current transport is driven by Loop Current ring shedding in the Gulf of Mexico. Using observations and eddy-permitting ocean model simulations, Mildner et al. (2013) showed a relationship between a ring shedding cycle of the Loop Current in the Gulf of Mexico and minima in FCT.

Chi et al. (2018) compared the FCT simulated by 13 numerical and reanalysis models with observations during 1993–2010. Annual values of FCT in 6 of the 13 models were correlated with observations at $p < 0.05$. Only 1 of the 13 models showed significant correlation with observations in winter (January–March), and none were correlated in spring (April–June), whereas 6 models in summer (July–September) and 9 models in autumn (October–December) showed significant correlation with observed FCT transport.

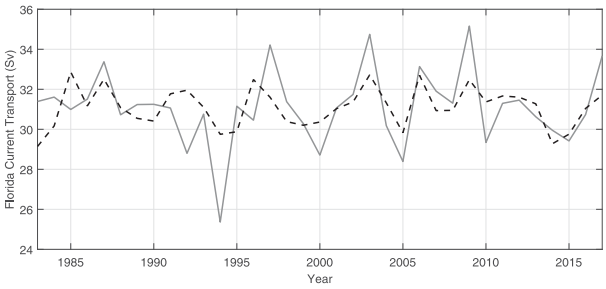

FIG. 1. Florida Current transport in the DJF season. The solid line is from observations, and the dashed line is a regression fit using the Icelandic low longitude and Azores high latitude with lag of 4 years as predictors.

2. Data and methods

a. Florida Current transport

FCT has been nearly continuously monitored via underwater cables and calibration cruises since 1982 (Larsen and Smith 1992; Meinen et al. 2010). We filled gaps in the cable observations using transport estimated from the cross-strait SSH difference, which is provided by the Atlantic Oceanographic and Meteorological Laboratory (Goni et al. 2017; Volkov et al. 2020). We calculated average transport for winter [December–February (DJF)], spring (March–May), summer (June–August), and autumn (September–November) for 1983–2017. The winter average is shown as a solid line in Fig. 1. The average DJF transport during this period was 31.1 Sv ($1\,\text{Sv} \equiv 10^6\,\text{m}^3\,\text{s}^{-1}$) with standard deviation of 1.9 Sv. These values are consistent with the annual mean and interannual variations of transport of 32 and 1–2 Sv, respectively, reported by Meinen et al. (2010) for 1964–2007. Analysis of FCT variations in spring, summer, and autumn seasons is the subject of ongoing studies and will be reported separately.

b. Centers of action

Figure 2 shows the mean wintertime (DJF) sea level pressure (SLP) over the North Atlantic for 1983–2017 from the NCEP–NCAR reanalysis (Kalnay et al. 1996). On this map, the

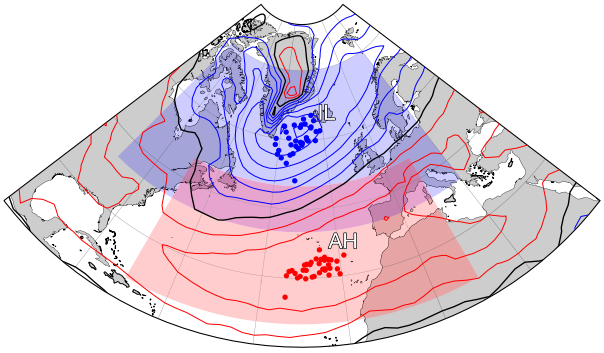

FIG. 2. Mean wintertime sea level pressure for 1983–2017. The black contour is 1014 hPa, the blue contours give values less than 1014 hPa with an interval of 3 hPa, and the red contours give values greater than 1014 hPa with an interval of 3 hPa. The regions used to define the Icelandic low (IL) and Azores high (AH) indices are indicated by the light blue and red shading, respectively. The blue and red dots give the locations of the centers of the IL and AH, respectively, in each year of the study. The 90% range for IL pressure is 1003.1–1021.0 hPa, and for the AH the range is 1016.8–1021.4 hPa. The latitude and longitude grids are every 15° beginning at 15°N and every 20° starting at 0°, respectively.

AH and the IL appear as extended irregularly shaped structures. To quantify their variations, objective indices for the pressure, latitude, and longitude locations for AH and IL were calculated using gridded SLP data as described by Hameed and Piontkovski (2004). By examining the monthly SLP maps since 1948 from NCEP to NCAR reanalysis SLP data, the latitude–longitude domains over which each of the pressure centers occurs were identified. The domain for the AH is 20°–50°N, 70°W–10°E; for the IL it is 40°–75°N, 90°W–20°E (shown in Fig. 2). The pressure index for each center of action (CoA) is defined as an area-weighted pressure departure from a threshold value over its domain and is therefore a measure of the anomaly of atmospheric mass over the domain. The location indices give pressure-weighted mean latitudinal and longitudinal positions of the centers. Note that the domains of the High and the Low overlap and the threshold that separates them is 1014 hPa. If the monthly averaged pressure in a grid box is greater than 1014 hPa, it is assigned to the AH and for a lower value to the IL. Hameed (2020) gives monthly values of the indices of atmospheric CoAs.

c. *ECCO state estimate*

To better understand the dynamical connection between atmospheric forcing and FCT, we apply wind stress perturbations to the ECCOv4 release-4 state estimate (Forget et al. 2015; Fukumori et al. 2020a,b). ECCOv4 is based on the MITgcm, has a nominal resolution of 1.0°, is available from 1992, and uses an adjoint method for data assimilation. As a dynamically consistent state estimate, ECCOv4 is free from the unphysical jumps and corrections typical of sequential reanalyses. It has been used for several studies of heat content and transport variability in the North Atlantic (e.g., Buckley et al. 2014, 2015; Piecuch et al. 2017; Jones et al. 2018). ECCOv4's representation of the Florida Current (mean transport and variability) is better than most available ocean reanalysis products, including those with much higher resolution (Chi et al. 2018).

ECCOv4 was initially chosen because we anticipated that variations in the background state would have a significant impact on the response of the circulation to wind forcing perturbations. If this were the case, having an accurate representation of the time evolution of the North Atlantic circulation would have been essential. Subsequent experimentation showed the response to be sufficiently robust that the choice of a specific model or reanalysis is unlikely to have a significant qualitative impact on the results.

3. The centers of action and their impact on ocean circulation

The IL and AH migrate stochastically along a southwest/northeast axis, with the IL migration path more inclined relative to latitude circles than the AH's path (Fig. 2). The associated pressure also fluctuates, with 90% of the pressure values falling between 1003.1 and 1021.0 and between 1016.8 and 1021.4 hPa for the IL and AH, respectively. The impact of these fluctuations on ocean circulation can be understood by considering the ocean wind stress and wind stress curl patterns associated with a 1-standard-deviation fluctuation of each of the CoA indices. The patterns shown in Figs. 3 and 4 were obtained by regressing each of the CoA indices against NCEP–NCAR reanalysis surface stress for the winters of 1983–2017. Note that while these patterns are *associated with* changes in the CoAs, we do not claim that these patterns are *caused by* changes in the CoAs. The positions and pressures of the IL and AH respond to hemisphere-to-planetary scale redistributions of atmospheric mass due to teleconnections and quasi-stationary planetary waves. On longer time scales, the CoAs also respond to changes in ocean circulation (Rossby 1939; Serreze et al. 1997; Seager et al. 2003; Cassou 2008). Similar to the NAO, the CoA indices are convenient low-dimensional representations of the dynamics of the atmosphere, although we argue that the six CoA indices are more complete and useful metrics than the single NAO index. Understanding the large-scale dynamics responsible for fluctuations of the CoAs is a subject of ongoing research.

The patterns for IL and AH latitude (Figs. 3a,b) are very similar since the IL and AH tend to move north and south in unison. This is reflected in the high correlation between the IL and AH latitude indices (Table 1). The AH pressure index is also strongly correlated with the IL and AH latitude indices (Table 1) and so the AH pressure pattern (Fig. 3d) also closely resembles both latitude patterns. The IL pressure pattern (Fig. 3c) resembles the negative of the AH pressure pattern (Fig. 3d) at high latitudes (north of 45°N) but the low latitude winds associated with IL pressure fluctuations are weaker than those associated with AH pressure fluctuations. Both latitude patterns, the AH pressure pattern, and—to a lesser extent—the IL pressure pattern look very much like the NAO pattern (Fig. 5), as might be expected from their correlations with the NAO (Table 1).

In contrast, the IL and AH longitude patterns are distinctly different from the NAO and the other CoA patterns (Fig. 4).

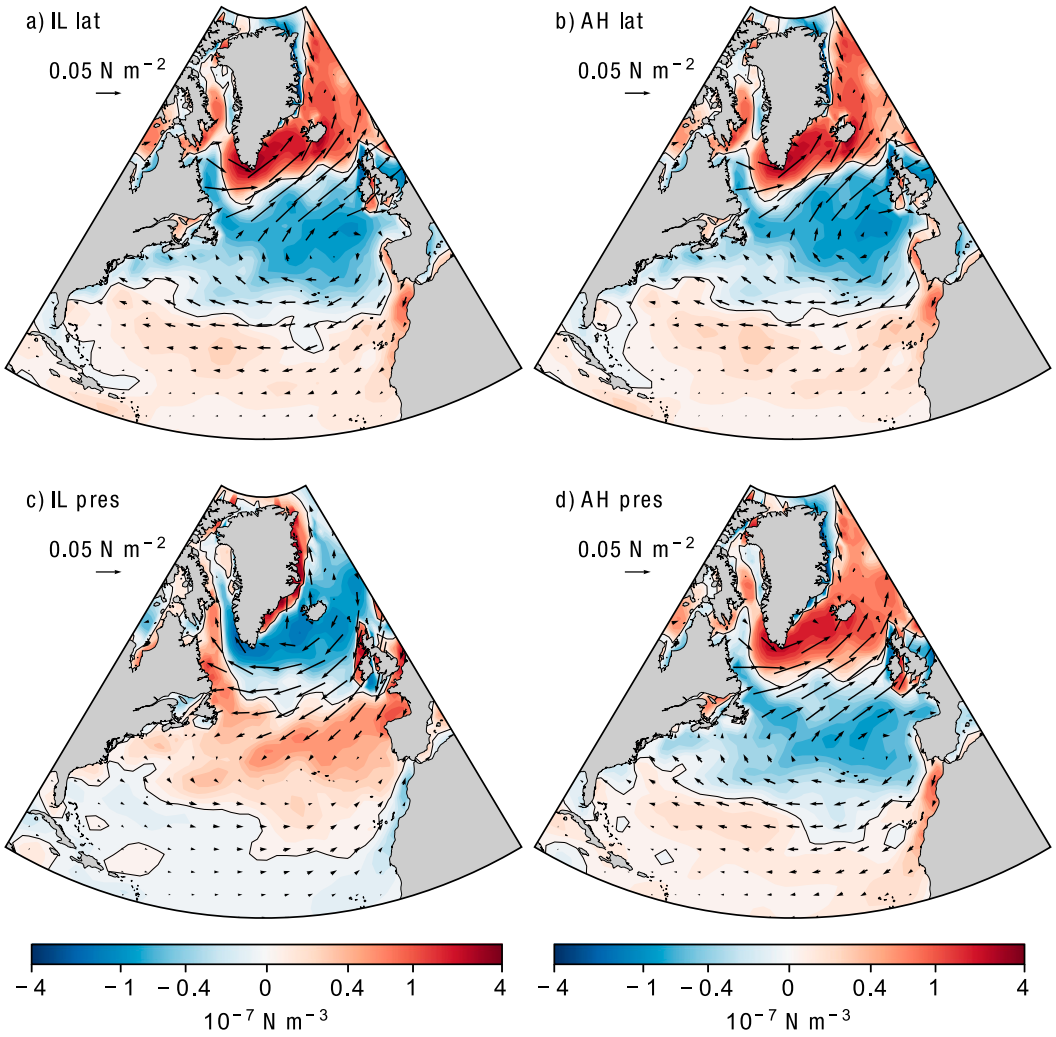

FIG. 3. Wind stress (arrows) and wind stress curl (shading) patterns associated with an index value of 1 standard deviation for IL (a) latitude and (c) pressure and AH (b) latitude and (d) pressure. A 1-standard-deviation change in the IL indices corresponds to a change of 4.2° of latitude or 2.9 hPa of pressure. For the AH, a 1-standard-deviation change in the indices corresponds to a change of 2.2° of latitude or 1.5 hPa of pressure. The color scale is logarithmic for wind stress curl values exceeding $\pm 5 \times 10^{-8}$ N m^{-3}, and the zero contour is given in black.

The AH longitude pattern (Fig. 4b) is dominated by a strong anticyclonic circulation centered just north of Iberia and cyclonic circulations around Greenland and south of the Canadian Maritimes; the cyclonic circulations drive winds parallel to the coast. The wind stress associated with the IL longitude (Fig. 4a) is oriented northwest/southeast at high latitudes—in contrast with the southwest/northeast orientation of the NAO, latitude, and pressure indices (Fig. 3)—and the wind stress off Nova Scotia and Newfoundland is stronger than in the other patterns. Both longitude patterns have negative (downwelling) wind stress curl anomalies near the North American coast. Farther offshore, the IL longitude wind stress curl pattern is negative north of a line running from Cape Cod to close to northwest Africa and positive (upwelling) south of this line. Conversely, the offshore wind stress curl pattern associated with AH longitude is positive south of Newfoundland (~47°N), becoming weak and finally negative off the southern tip of Florida.

Given their resemblance to the NAO pattern, the oceanic response to latitude and pressure fluctuations can be understood in much the same way as the NAO (e.g., Marshall et al. 2001). Namely, the associated wind stress patterns lead to a meridional shift in the wind stress curl pattern relative to the climatological pattern, which leads to a north/south migration of the intergyre boundary. Such shifts have been associated with meridional migrations of the Gulf Stream Extension (Taylor and Stephens 1998; Pérez-Hernández and Joyce 2014; Wolfe et al. 2019) and changes to the formation rate of subtropical mode water (Joyce et al. 2000).

The effect of changes in the CoA longitude indices is distinctly different from that of the NAO and the intraseasonal response of the Florida Current is greatly influenced by the

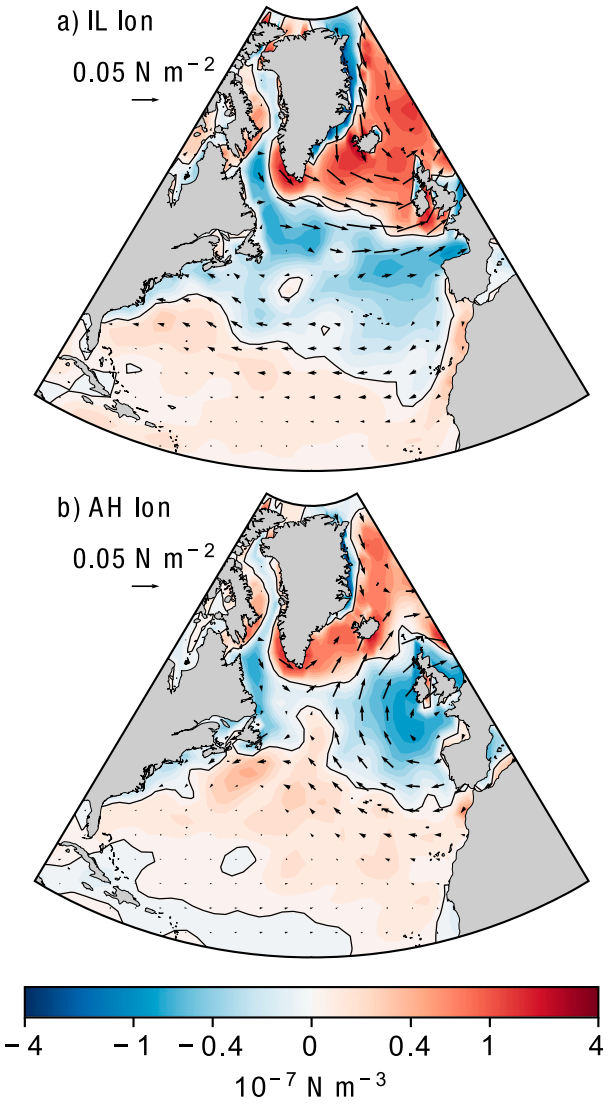

FIG. 4. As in Fig. 3, but for (a) IL and (b) AH longitude. A 1-standard-deviation change in the IL and AH longitude indices corresponds to 12° and 6.1°, respectively.

nearshore winds. On short time scales, the ocean's response to wind forcing is primarily barotropic and may be understood using the barotropic potential vorticity equation,

$$\frac{DQ}{Dt} = \hat{k} \cdot \nabla \times \frac{\boldsymbol{\tau}}{H} = \frac{1}{H} \hat{k} \cdot \left(\frac{\boldsymbol{\tau} \times \nabla H}{H} + \nabla \times \boldsymbol{\tau} \right),$$

where Q is the barotropic potential vorticity, $\boldsymbol{\tau}$ is the wind stress, and $\hat{k}$ is the unit vector in the vertical direction. This equation shows that the effect of wind forcing is greatest where the wind stress curl is large (the second term in parentheses) and where the wind blows along steeply sloping isobaths (the first term in parentheses). Near the coast, bathymetry is steepest near the shelfbreak, which we approximate here as the 200-m isobath and refer to the components of the wind along and across this isobath as longshore and cross-shore,

TABLE 1. Correlations between the IL pressure, longitude, and latitude indices; the AH pressure, longitude, and latitude indices; and the NAO. The correlations are in the DJF season during 1983–2017. Statistically significant correlations at $p < 0.05$ are shown in boldface type.

	IL-Lon	IL-Pres	AH-Lat	AH-Lon	AH-Pres	NAO
IL-Lat	**0.43**	**−0.49**	**0.91**	**0.38**	**0.79**	**0.92**
IL-Lon		**−0.43**	0.29	0.12	**0.46**	**0.45**
IL-Pres			−0.27	−0.14	**−0.69**	**−0.70**
AH-Lat				**0.50**	**0.67**	**0.82**
AH-Lon					0.32	**0.47**
AH-Pres						**0.90**

respectively. As shown in Fig. 6, the longshore winds associated with both the IL and AH longitude indices are predominantly downwelling-favorable (logically southward, negative values in Fig. 6) south of the Grand Banks of Newfoundland (south of ~4500 km in Fig. 6) and upwelling-favorable for a distance of 500–1000 km north of this point. A major difference between the IL and AH longitude patterns is that the AH longitude winds change sign off the Florida coast to become upwelling-favorable (Fig. 6c) while the IL longitude winds remain weakly downwelling-favorable (Fig. 6b).

Farther offshore, as seen in Fig. 4, the wind stress curl pattern related to IL longitude is associated with a broad swath of anticyclonic curl (for positive index values) running southeast across the midlatitude North Atlantic that is flanked to the north and south by regions of oppositely signed curl. In contrast, the curl associated with AH longitude is mostly single signed between 18° and 45°N. This means that changes in AH longitude drive circulation anomalies of the same sign

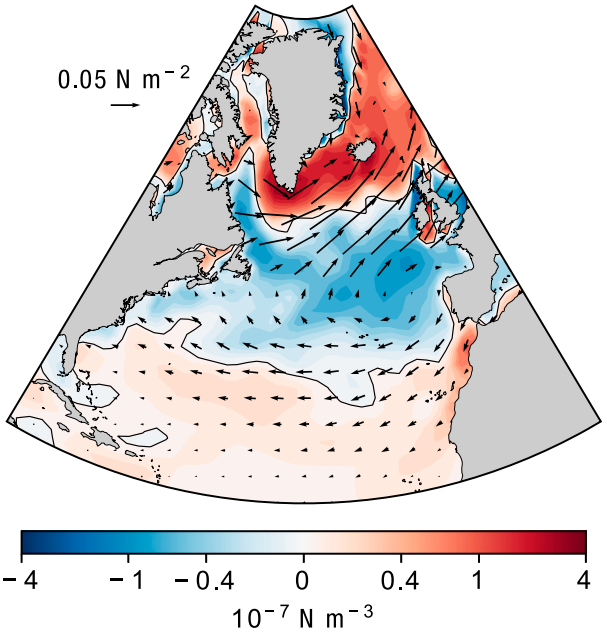

FIG. 5. As in Fig. 3, but for the wintertime NAO (DJF PC-based Hurrell index; Hurrell 1995).

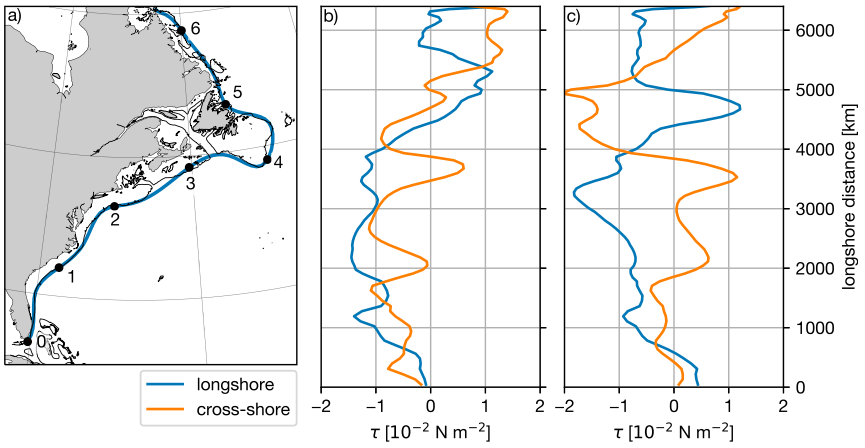

FIG. 6. The longshore (blue) and cross-shore (orange) wind stress along the (a) thick blue curve for a 1-standard-deviation value of the (b) IL and (c) AH longitude indices. Positive cross-shore wind stress is oriented offshore; positive longshore is 90° to the left of offshore. The curve in (a) follows the 200-m isobath (shown as a thin black contour) but is simplified and smoothed to highlight large-scale features. The labeled dots in (a) give the longshore distance along the path in units of 1000 km.

throughout the subtropical gyre, whereas changes in IL longitude drive anomalies that have opposite signs on either sign of the wind stress curl line extending from the U.S. mid-Atlantic states to northwest Africa.

4. Effect of the centers of action on Florida Current transport

Table 2 lists correlation coefficients between FCT and the NAO, the IL pressure, longitude, and latitude, and AH pressure, longitude and latitude in winter (DJF) with lags up to 4 years. The statistical significance of each correlation coefficient was estimated by the random phase method of Ebisuzaki (1997). In Table 2 we see that FCT is not significantly correlated with the NAO index, but that there are statistically significant correlations with IL longitude at zero lag and the latitudes of the AH and IL with a lag of 4 years.

a. Impact of Icelandic low longitude

Here we consider physical processes that can give rise to the correlation of FCT with IL longitude position with zero lag. The correlation coefficient is −0.50, which means 25% of the interannual variations of FCT in winter are related to zonal movements of the IL. A related question of interest is why variations of IL pressure or latitude are not correlated with FCT.

1) REGRESSION ANALYSIS

To investigate these questions, we regress FCT against wind stress and wind stress curl over the North Atlantic from the NCEP–NCAR reanalysis. The pattern (Fig. 7a) bears a strong resemblance to the (negative of the) pattern produced by IL longitude (Fig. 4a), typified by upwelling-favorable longshore winds along the southern Canadian Maritimes, New England, and the Carolinas and downwelling-favorable longshore winds on the coasts of Labrador and eastern Newfoundland. The wind stress curl pattern extended from Labrador to Iberia associated with the FCT is also similar to that seen in the IL longitude pattern, although the FCT wind stress curl zero line is more irregular and is shifted northward relative to the IL longitude pattern.

The correlation between FCT and IL longitude and their associated wind stress and curl patterns suggests that the FCT's correlation with IL longitude is a response to the associated wind stress anomalies. In particular, we hypothesize that the longshore wind stress on the North American coast creates coastal sea level anomalies that propagate as coastal trapped waves to the Straits of Florida and affect transport by reducing or enhancing the sea surface slope across the Straits. This mechanism is very similar to that proposed by Czeschel et al. (2012) to explain the annual cycle of FCT. Here, we show that this mechanism drives interannual variability as well.

TABLE 2. Correlations between Florida Current transport and the NAO; the IL pressure, longitude, and latitude; and the AH pressure, longitude, and latitude. The correlations are in the DJF season during 1983–2017. Statistically significant correlations at $p < 0.05$ are shown in boldface type.

	Lag (years)				
	0	1	2	3	4
NAO	−0.18	−0.23	0.02	0.18	0.23
IL-Pres	0.20	0.23	0.06	0.05	0.10
IL-Lon	**−0.50**	−0.09	0.26	0.22	0.25
IL-Lat	−0.14	−0.23	−0.03	0.06	**0.37**
AH-Pres	−0.14	−0.05	0.02	0.04	0.23
AH-Lon	−0.07	−0.01	−0.22	−0.05	0.24
AH-Lat	−0.15	−0.07	−0.10	0.01	**0.47**

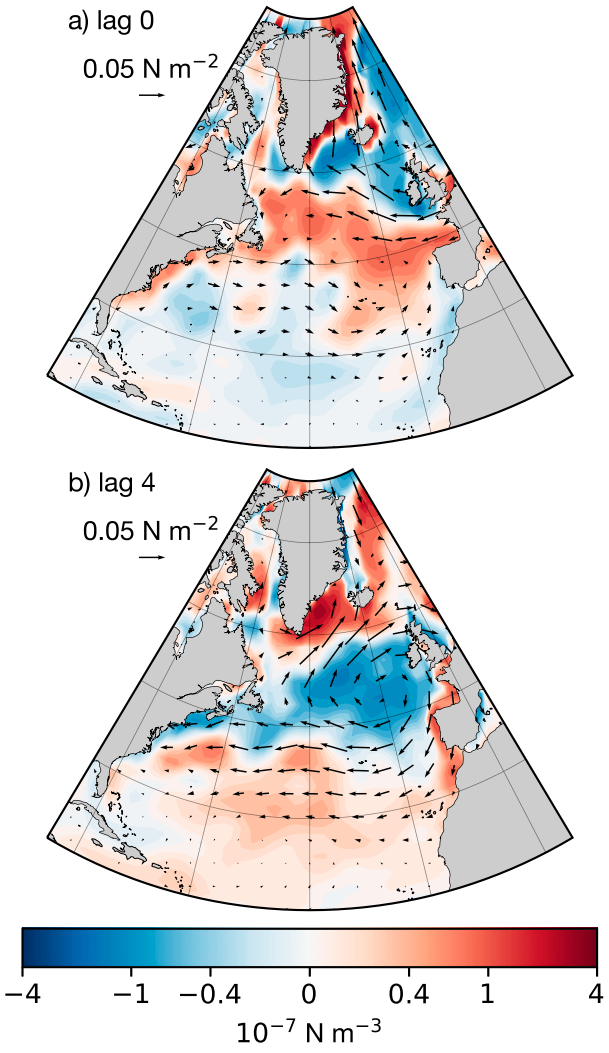

FIG. 7. Wind stress (arrows) and wind stress curl (shading) patterns associated with a $+2\sigma$ value of wintertime FCT with FCT lagging the atmosphere by (a) 0 and (b) 4 years. The color scale is logarithmic for wind stress curl values exceeding $\pm 5 \times 10^{-8}$ N m^{-3}.

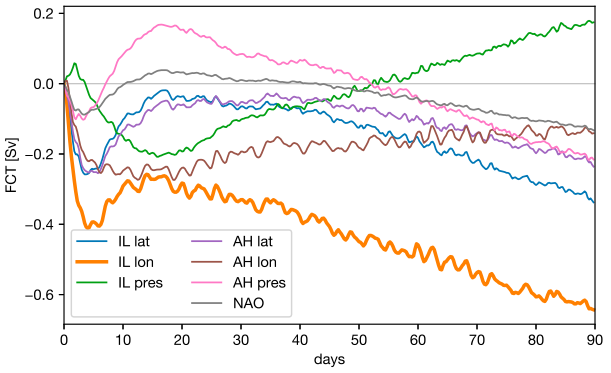

FIG. 8. Anomaly of FCT as a function of days since 1 Dec 1993, in response to wind stress perturbations associated with a 2-standard-deviation value of the IL and AH indices (see Figs. 3 and 4 for wind stress pattern) and a 2-standard-deviation value of the NAO (see Fig. 5 for wind stress pattern). The perturbations were ramped up linearly over 24 h and then held constant for 89 days. The IL longitude (thick orange line) produces the largest response at both early and late times.

2) PERTURBATION EXPERIMENTS

To test our hypothesis, we performed a series of experiments using the ECCOv4 model where wind stress perturbations corresponding to 2 standard deviations of the CoA indices and the NAO (i.e., 2 times what is shown in Figs. 3 and 4) were added to the model's original wind stress fields during the winter. The perturbation was ramped up linearly over 24 h beginning 1 December and held constant for the next 89 days. Linearly ramped wind forcing can, in principle, excite oscillations near the inertial period—these oscillations appear to be rapidly damped, and no significant near-inertial signal was seen in the response to the perturbations. Experiments in which the forcing was ramped up over four days rather than one produced nearly identical results except for a 3-day lag in the maximum response. Further experiments showed that the response to perturbations applied in different years was essentially identical, so the present discussion focuses on perturbations applied beginning December 1993. The response was also linear in magnitude for all perturbations tried (up to eight times larger than those shown Figs. 3 and 4), so we concentrate on perturbations corresponding to positive values of the CoA and NAO indices. The response to negative values can be obtained by multiplying all the results by −1. In the following, all fields shown are anomalies obtained by subtracting the (evolving) model state obtained using unperturbed forcing from that obtained using the perturbed winds.

The response of FCT to the wind stress perturbations is shown in Fig. 8. Consistent with the correlation analysis, IL longitude produces the largest response at both early and late times. The response to IL longitude rapidly increases to a temporary maximum at 5 days, reduces slightly over the next 10 days, and then steadily increases after 15 days. The response presumably eventually saturates, but on a time scale longer than a season. The nature of the final saturated state is not likely to be physically relevant since there is no plausible mechanism that would hold the perturbation forcing constant for so long.

The response of FCT to the other indices is similar to that of IL longitude—an initial transient lasting about 2 weeks followed by a transition to steady drift—but the magnitude of the responses is smaller. The response to AH longitude comes close in magnitude to that of the response to IL longitude but begins to decay after about 20 days. Interestingly, the NAO produces the weakest response of all the indices.

The net wind stress curl anomaly associated with the IL and AH longitude perturbations is smaller than those of the other perturbations in the region east of the Straits of Florida and over extent of the subtropical gyre (Figs. 3 and 4). This means that the response of the Florida Current to these perturbations is not simply due to a spinup or spindown of the gyre circulation in response to changes in the wind stress curl. Instead, the dynamical response of the Florida Current to the IL and AH

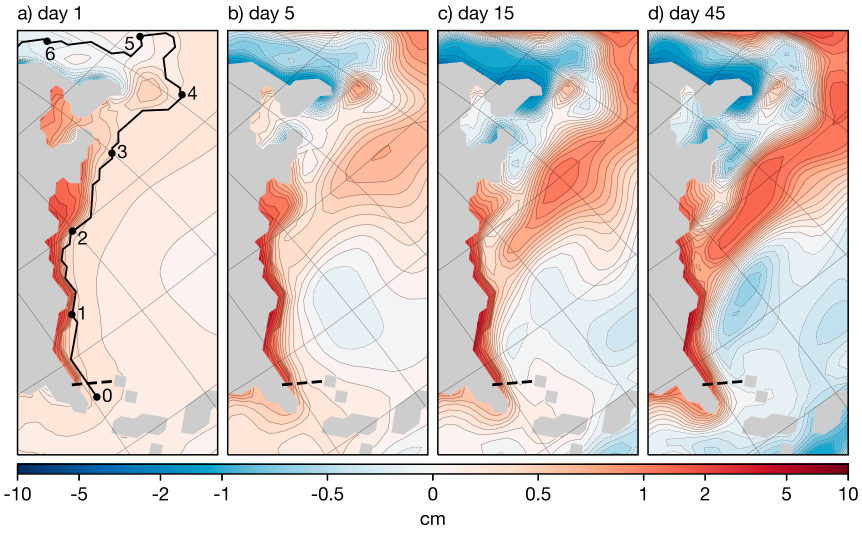

FIG. 9. Anomaly of SSH (cm) near the east coast of North America (a) 1, (b) 5, (c) 15, and (d) 45 days after application of wind stress anomalies associated with a 2-standard-deviation value of IL longitude. The color scale is logarithmic for values exceeding ±1 cm, and the grid has been rotated to make the coast approximately vertical. The model's representation of land is shaded gray, and the Straits of Florida section is indicated by a black dashed line. The solid black line in (a) gives the longshore section used for the Hovmöller plot in Fig. 10 (below), with distance along the section labeled in units of 1000 km.

longitude perturbations is most easily understood by considering the evolution of anomalous sea surface height (SSH), which is related to surface currents through geostrophy. Figure 9 shows the evolution of SSH (with the effects of ice loading removed) under IL longitude forcing near the North American east coast as a sequence of snapshots and Fig. 10a shows the evolution of SSH at the Straits of Florida. (For a basinwide view, see Fig. S1 in the online supplemental material.) The first effect of the wind is direct setup of the coastal sea level south of Newfoundland (Fig. 9a) due to a combination of downwelling-favorable winds and the frictional response to onshore winds (Fig. 6b). Along the north coast of Newfoundland and Labrador, the winds have the opposite sense and drive coastal sea level down (Fig. 9a). The sea level is also high farther offshore due to the negative wind stress curl forcing south and east of Nova Scotia and Newfoundland (Fig. 4a). This high sea level signal extends down the entire U.S. coast, presumably propagated by a deep-water Kelvin wave. [It is difficult to observe the propagation of such a wave using the 6-hourly data that were saved since such waves would travel at speeds of 200 m s^{-1} and cross-shore scales of 2000 km in water 4000 m deep (e.g., Gill 1982, section 10.4).]

By day 5, this broad region of high SSH has become concentrated on the shelf between south Florida and Nova Scotia, further raising coastal sea level relative to its offshore value. FCT briefly peaks (cf. Fig. 8) at this time because of the SSH gradient across the Straits of Florida (Fig. 9b). The positive wind stress curl forcing offshore of the South Atlantic Bight (SAB) has produced an SSH low offshore, but this low only has a small effect on SSH at the Straits of Florida (Fig. 10a) and does not substantially affect FCT. The low sea level along the Labrador Coast has also begun to migrate around the Grand Banks to produce a trough between offshore and the large-scale high southeast of Nova Scotia (prominent in the upper-left quarter of Fig. 9b) and the high coastal sea level. This feature continues to propagate down the coast toward Florida but is more distinct as a bottom pressure signal than in SSH (Fig. 11). Since the difference between bottom pressure and SSH anomalies is proportional to the vertically integrated density anomaly, this is an indication that the associated waves are baroclinic in character. The waves propagate along the black line shown in Fig. 9a, which follows a contour of f/H that passes through the Straits of Florida. The evolution of bottom pressure along this path, shown in Fig. 11, reveals that the northern upwelling signal propagates down the coast toward Florida at approximately 6.5 cm s^{-1}. The later waves do not appear to make it past Cape Hatteras (at ~1500 km in Fig. 11), but the earlier waves do and arrive at the Straits of Florida between days 5 and 10. The arrival of these waves corresponds to the temporary reduction in the magnitude of the FCT anomaly (Fig. 8). After the arrival of the waves, the FCT anomaly is surface intensified whereas before it was dominantly barotropic (not shown).[1] While detailed diagnosis of these waves is beyond the scope of this study, their propagation speed and direction are consistent with baroclinic coastal-trapped waves (e.g., Brink 1991).

After about 10 days, the SSH low off the SAB has moved slightly west and begins to play a dominant role in setting the

[1] Only the anomaly is barotropic—the Florida Current in both the background and perturbed runs is strongly baroclinic.

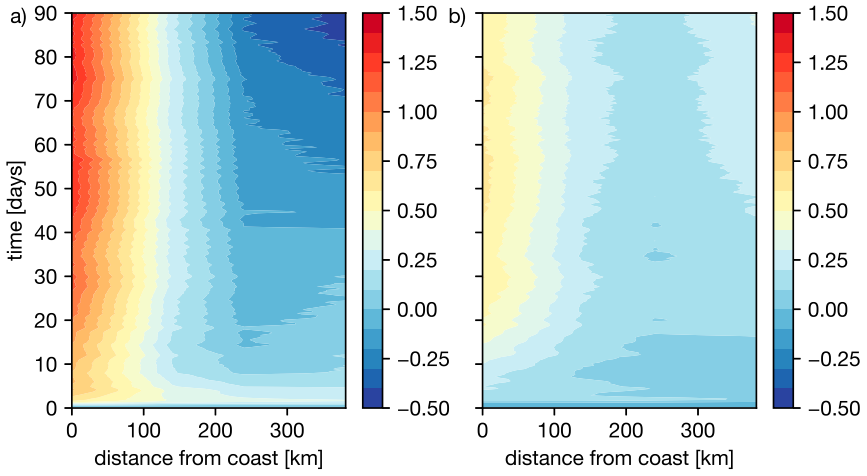

FIG. 10. Anomaly of SSH (cm) as a function of distance from the coast along the Straits of Florida section and time since the initiation of wind stress perturbations associated with the (a) IL and (b) AH longitude indices.

sea level in the eastern half of the Florida Current section (Fig. 10a) while the coastal sea level high continues to build, possibly due to the curl-driven SSH high centered southeast of Newfoundland that connects to the coast near Cape Hatteras (Fig. 9c). After about day 15–20, the magnitude of the FCT anomaly begins its long-term growth trend (Fig. 8) in response to westward-propagating, curl-driven interior SSH anomalies (Fig. 9d) that continue to raise coastal sea level while depressing the sea level in the eastern half of Florida Current section (Fig. 10a).

The initial coastal response of SSH to AH longitude perturbations is similar to the previously discussed IL longitude case, except that the coastal sea level is high rather than low north of Newfoundland (cf. Fig. 12a with Fig. 9a; see also Fig. S2 in the online supplemental material) and the coastal response off south Florida is weaker due to the upwelling favorable winds at this latitude (Fig. 6c). This latter feature means that the sea level gradient at the Straits of Florida is weaker (Fig. 10a) and the growth of FCT is slower (Fig. 8) at early times relative to the response to the IL longitude perturbation. An additional difference is that the sea level offshore of the entire east coast is low due to the positive offshore wind stress curl anomaly (Fig. 4b). As time progresses, the curl-driven SSH low offshore between northern Florida and Nova Scotia intensifies and moves westward (Fig. 12). The combination of upwelling-favorable winds off south Florida and the influence of the offshore low limit the growth of sea level anomalies at the coast (Fig. 10b). At later times, the weakly negative wind stress curl south of Florida (Fig. 4b) creates a sea level high centered on Cuba (Figs. 12c,d) that limits the influence on the Florida Current section of the offshore low to the north. As a result of these factors, the coastal sea level at the Florida Current section never gets as high and the offshore sea level never gets as low as in the IL longitude case. The SSH gradient across the Straits of Florida and, consequently, the FCT anomaly therefore remain weak as compared with the IL longitude case.

The above discussion focuses on the effect of winds near the North American coast and immediately offshore, with the implicit assumption that local winds are the most important factor driving the response of FCT to IL longitude. To verify this assumption, we performed an addition perturbation experiment using only the component of the IL longitude wind stress pattern near the North American coast stretching from the Greater Antilles to Newfoundland. The wind stress pattern is shown in Fig. 13 and the response of FCT in Fig. 14.

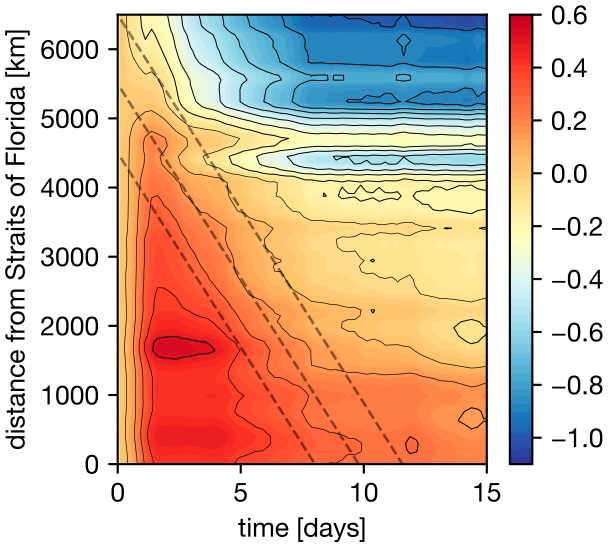

FIG. 11. Hovmöller diagram of bottom pressure anomaly divided by $\rho_0 g$ (cm) along the line shown in Fig. 9a as a function of time since the initiation of the perturbation shown in Fig. 9 and longshore distance. The heavy dashed lines give a propagation speed of 6.5 cm s^{-1} down the coast (toward the Straits of Florida). The nearest-neighbor interpolation used to extract this field from the model output results in gridscale noise that was removed by two applications of a 1–2–1 filter.

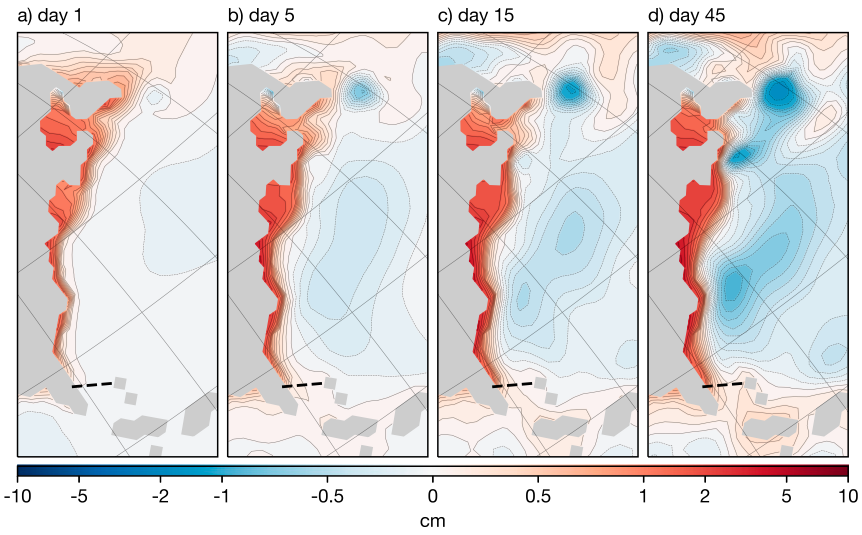

FIG. 12. As in Fig. 9, but for the wind stress pattern associated with the AH longitude.

The response to this restricted wind stress perturbation is nearly identical to that to the full IL longitude wind stress pattern, except that the local minimum around day 15 is missing because the pattern shown in Fig. 13 does not produce upwelling north of Newfoundland. In addition to longshore winds, this perturbation has region of negative wind stress curl south and southeast of Newfoundland that produces an interior downwelling signal sufficient to sustain the steady long-term growth in FCT. The online supplemental material shows animations of sea surface height near the coast in response to the IL longitude and AH longitude wind stress perturbations.

b. *Impact of Icelandic low and Azores high latitude*

In Table 2, we also see that FCT is correlated with latitudinal movements of both the Azores high and the Icelandic low with a lag of 4 years. To understand this result, we regressed FCT transport and wind stress 4 years earlier—the results are shown in Fig. 7b. The overall pattern is similar to the patterns associated with AH and IL latitude, and shares the region of positive wind stress curl east of the Straits of Florida near 30°N seen in the CoA latitude patterns but *not* in the pressure or NAO patterns (Figs. 3a,b, and 5; see also Fig. 12). Baroclinic Rossby wave propagation from this region to the Straits of Florida has been suggested as a mechanism for perturbing FCT transport by several authors (DiNezio et al. 2009; Czeschel et al. 2012; Frajka-Williams et al. 2013; Domingues et al. 2016, 2019).

In the adjoint model calculations of Czeschel et al. (2012), long baroclinic Rossby waves from east of Florida were important contributors to forcing of FCT. First mode baroclinic planetary waves propagated westward to Straits of Florida, but the magnitude of their contribution is highly sensitive to topography. The phase speed of these waves was 3.7 cm s^{-1}. In Fig. 5b we see that FCT transport is correlated with wind stress curl over the ocean east of Florida from about 60°W to the African coast.

We calculated the coefficient of determination r^2 (i.e., square of correlation coefficients) of wind stress curl in the subtropical Atlantic with AH latitude; these are presented in Fig. 15. If we consider westward propagation of the first mode baroclinic waves contributing to the perturbation of FCT transport, then a travel time of 4 years would place the average location of the origin of these waves near 35°W where a region of maximum correlations with r^2 between 0.3 and 0.4 is seen. Distribution of r^2 of IL latitude with wind stress curl (not shown) is similar to that in Fig. 12 because IL latitude and AH latitude are highly correlated with $r = 0.91$ (Table 1).

Riemer et al. (2006) showed that easterly winds from Africa in the subtropical latitudes in the winter season are modulated by north–south shifts of the Azores high (Fig. 3 in their paper). Easterly winds are strong when the AH migrates to an anomalously northward position. When the AH shifts to the south it blocks airflow resulting in weaker winds from the east.

In Fig. 9 of Czeschel et al. (2012), second mode Rossby waves are shown to originate from an area extending from the Grand Banks to the east of the Mid-Atlantic Ridge and reaching the Florida coast in 4 years. This is consistent with the result in Fig. 7b that FCT is significantly correlated with wind stress curl in this region 4 years earlier. We note that adjoint sensitivities are different from the correlations. A region of high sensitivity does not necessarily imply a high correlation. However, the consistency of the two methods is noteworthy. Czeschel et al. (2012) suggest that these waves are not directly wind-forced but are produced by bottom current variations interacting with topography. However, bottom-current variations are ultimately wind-driven, since the sensitivity is to the wind forcing, but the precise pathway between the wind and topography were not determined in that study. This source region of second mode waves identified in the model of Czeschel et al. (2012) and their propagation to the southwest is consistent with satellite observations of Osychny and Cornillon (2004), who suggested an interaction of the Gulf Stream with

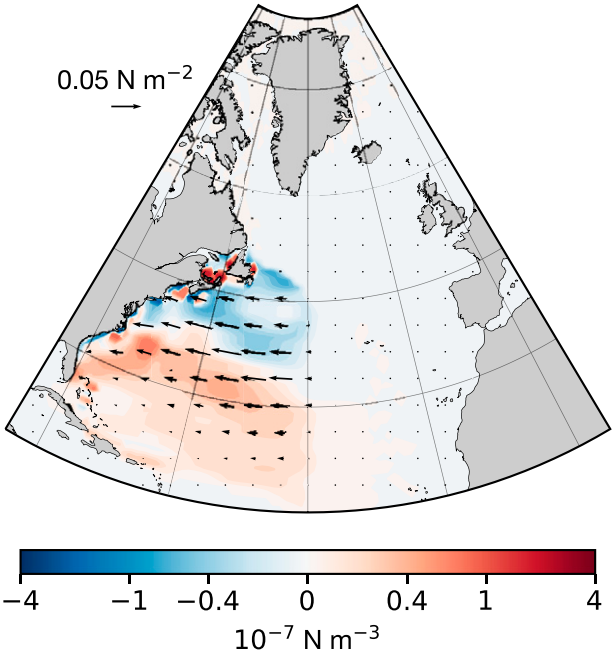

FIG. 13. Wind stress (arrows) and wind stress curl (shading) patterns for the "coastal wind" perturbation.

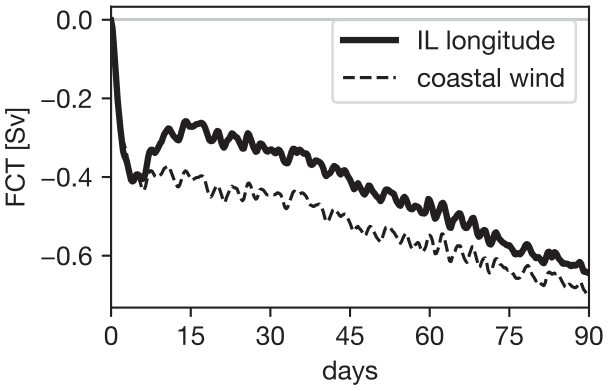

FIG. 14. Anomaly of FCT as a function of days since 1 Dec 1993, in response to the wind stress perturbation associated with a 2-standard-deviation value of the IL longitude (solid) and the coastal-wind stress perturbation (dashed). See Fig. 4a for the IL longitude perturbation and Fig. 9 for the coastal-wind perturbation. The perturbations were ramped up linearly over 24 h and then held constant for 89 days.

the bottom topography south of the Grand Banks as source for the waves.

Movements of IL longitude and AH latitude 4 years earlier are linearly independent—the correlation between them is statistically insignificant ($r = -0.14$). We therefore developed a linear regression model for FCT transport using these two independent variables:

$$\mathrm{FCT}(t) = -0.13\,\mathrm{IL}_{\mathrm{Lon-DJF}}(t) + 0.20\,\mathrm{AH}_{\mathrm{Lat-DJF}}(t-4) + 20.45,$$

This regression explains 29% of DJF FCT variance. Its prediction of FCT is shown as the dashed line in Fig. 1. The regression is statistically significant with the F ratio of 6.5.

5. Conclusions

This paper has presented evidence that interannual variations of Florida Current transport in winter are influenced by displacements of the Icelandic low and the Azores high. These pressure centers migrate zonally and meridionally resulting in shifts in the distribution of wind stress at the ocean surface.

The zonal movement of the Icelandic low is related to the Florida Current within the same season, without a significant lag. Perturbation experiments with ECCOv4 model show that the correlation between Florida Current transport and IL longitude is a response to the associated wind stress anomalies. In particular, the wind stress near the North American coast creates coastal and offshore sea level anomalies that affect transport by reducing or enhancing the sea surface slope across the Straits.

Florida Current transport is also impacted by meridional shifts of the Azores high and the Icelandic low with a lag of 4 years. Latitude variations of these pressure centers are highly correlated (Table 1) and therefore perturbation of wind stress curl by variations in the latitudes of both are similar (Figs. 3a,b). Both show extensive positive wind stress curl anomalies in the ocean east of Straits of Florida. Baroclinic planetary wave propagation from this region to the Straits of Florida has been suggested as a mechanism for perturbing FCT transport by several authors (DiNezio et al. 2009; Czeschel et al. 2012; Frajka-Williams et al. 2013; Domingues et al. 2016, 2019). Wind stress perturbations in these regions are likely to be related with latitudinal movements of the Azores high because easterly winds from Africa are strong when the AH shifts to the north and the winds are weak when the AH shifts southward and blocks their flow (Riemer et al. 2006). Variations in the latitudes of the Icelandic low and the Azores high are correlated with negative anomalies in wind stress curl east of the Grand Banks 4 years later (Figs. 3a,b). This region has been identified in the model studies of Czeschel et al. (2012) as a source of Rossby waves that reach Florida states in 4 years.

A recent paper by Kostov et al. (2021) uses the ECCOv4 output to identify sources of variability in the AMOC in RAPID-MOCHA data at 26°N and also in OSNAP data at

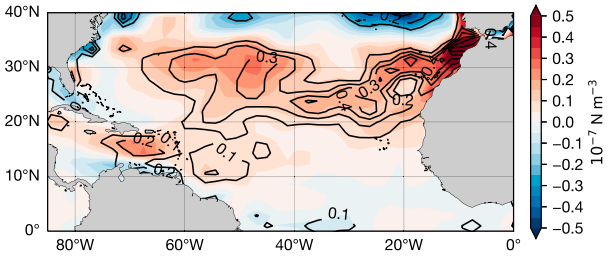

FIG. 15. Wind stress curl associated with a 1-standard-deviation variation of AH latitude (color shades) and fraction of wind stress curl variations explained by AH latitude (r^2; contours). The contour interval is 0.1.

53°N. but making use of adjoint sensitivities in the MITgcm. They find a sensitivity of overturning at 26°N to northward wind stress along the American Coast, similar to our results in section 4a. Kostov et al. (2021) also find that Rossby waves from the ocean to the east play an important role in perturbing transport through 26°N, as we report in section 4b. These findings are similar to those reported by Czeschel et al. (2012) who used the adjoint of MITgcm to identify the factors driving the seasonal cycle of the Florida Current. As the Florida Current is a significant component of the AMOC at 26°N (e.g., McCarthy et al. 2015), similarities between in their sensitivities to wind stress anomalies are to be expected. The analysis presented in this paper shows that the wind stress perturbations along the American Coast are associated with longitudinal displacement of the Icelandic low, and latitudinal displacements of the Azores high's perturbation of wind stress in the subtropical North Atlantic result in westward wave propagation that alters Florida Current transport.

This paper has focused on interactions of Florida Current with the Icelandic low and the Azores high in the winter season. The locations and strengths of the atmospheric centers of action have large variations with season. Hence, the distribution of wind stress over the ocean also changes substantially from season to season. Correlations between Florida Current transport and the Icelandic low and Azores high pressures and positions are different, and occur at different lags in winter, spring, summer and autumn. Each requires in-depth investigation to unravel its dynamical pathway. We expect to pursue these relationships in future work.

Acknowledgments. This work is supported by NSF Grant OCE-1634829. Much of the analysis was performed using the Python Scientific Stack (NumPy, SciPy, Pandas, XArray, MatPlotLib, and Cartopy). Analysis of the ECCOv4 results was facilitated by the Python packages xmitgcm, xgcm, and ecco_v4_py.

Data availability statement. Daily data for FCT are available from the website of the Florida Transport Project (https://www.aoml.noaa.gov/phod/floridacurrent/index.php). The NAO index is available from NCAR (https://climatedataguide.ucar.edu/climate-data/hurrell-north-atlantic-oscillation-nao-index-pc-based). The data for the Icelandic low and the Azores high are available at the corresponding author's website (https://you.stonybrook.edu/coaindices).

REFERENCES

Anderson, D. L. T., and R. A. Corry, 1985a: Ocean response to low frequency wind forcing with application to the seasonal variation in the Florida Straits–Gulf Stream transport. *Prog. Oceanogr.*, **14**, 7–40, https://doi.org/10.1016/0079-6611(85)90003-5.

——, and ——, 1985b: Seasonal transport variations in the Florida Straits: A model study. *J. Phys. Oceanogr.*, **15**, 773–786, https://doi.org/10.1175/1520-0485(1985)015<0773:STVITF>2.0.CO;2.

Bakalian, F., S. Hameed, and R. Pickart, 2007: Influence of the Icelandic Low latitude on the frequency of Greenland tip jet events: Implications for Irminger Sea convection. *J. Geophys. Res.*, **112**, C04020, https://doi.org/10.1029/2006JC003807.

Baringer, M. O., and J. C. Larsen, 2001: Sixteen years of Florida Current transport at 27°N. *Geophys. Res. Lett.*, **28**, 3179–3182, https://doi.org/10.1029/2001GL013246.

Barnston, A. G., and R. E. Livezey, 1987: Classification, seasonality and persistence of low-frequency atmospheric circulation patterns. *Mon. Wea. Rev.*, **115**, 1083–1126, https://doi.org/10.1175/1520-0493(1987)115<1083:CSAPOL>2.0.CO;2.

Brink, K. H., 1991: Coastal-trapped waves and wind-driven currents over the continental shelf. *Annu. Rev. Fluid Mech.*, **23**, 389–412, https://doi.org/10.1146/annurev.fl.23.010191.002133.

Buckley, M. W., R. M. Ponte, G. Forget, and P. Heimbach, 2014: Low-frequency SST and upper-ocean heat content variability in the North Atlantic. *J. Climate*, **27**, 4996–5018, https://doi.org/10.1175/JCLI-D-13-00316.1.

——, ——, ——, and ——, 2015: Determining the origins of advective heat transport convergence variability in the North Atlantic. *J. Climate*, **28**, 3943–3956, https://doi.org/10.1175/JCLI-D-14-00579.1.

Cassou, C., 2008: Intraseasonal interaction between the Madden–Julian Oscillation and the North Atlantic Oscillation. *Nature*, **455**, 523–527, https://doi.org/10.1038/nature07286.

Chi, L., C. L. P. Wolfe, and S. Hameed, 2018: Intercomparison of the Gulf Stream in ocean reanalyses: 1993–2010. *Ocean Modell.*, **125**, 1–21, https://doi.org/10.1016/j.ocemod.2018.02.008.

Czeschel, L., C. Eden, and R. J. Greatbatch, 2012: On the driving mechanism of the annual cycle of the Florida Current transport. *J. Phys. Oceanogr.*, **42**, 824–839, https://doi.org/10.1175/JPO-D-11-0109.1.

DiNezio, P. N., L. J. Gramer, W. E. Johns, C. S. Meinen, and M. O. Baringer, 2009: Observed interannual variability of the Florida Current: Wind forcing and the North Atlantic Oscillation. *J. Phys. Oceanogr.*, **39**, 721–736, https://doi.org/10.1175/2008JPO4001.1.

Domingues, R. M., M. Baringer, and G. Goni, 2016: Remote sources for year-to-year changes in the seasonality of the Florida Current transport. *J. Geophys. Res. Oceans*, **121**, 7547–7559, https://doi.org/10.1002/2016JC012070.

——, W. E. Johns, and C. S. Meinen, 2019: Mechanisms of eddy-driven variability of the Florida Current. *J. Phys. Oceanogr.*, **49**, 1319–1338, https://doi.org/10.1175/JPO-D-18-0192.1.

Ebisuzaki, W., 1997: A method to estimate the statistical significance of a correlation when the data are serially correlated. *J. Climate*, **10**, 2147–2153, https://doi.org/10.1175/1520-0442(1997)010<2147:AMTETS>2.0.CO;2.

Forget, G., J.-M. Campin, P. Heimbach, C. Hill, R. Ponte, and C. Wunsch, 2015: ECCO version 4: An integrated framework for non-linear inverse modeling and global ocean state estimation. *Geosci. Model Dev.*, **8**, 3071–3104, https://doi.org/10.5194/gmd-8-3071-2015.

Frajka-Williams, E., W. Johns, C. Meinen, L. Beal, and S. Cunningham, 2013: Eddy impacts on the Florida Current. *Geophys. Res. Lett.*, **40**, 349–353, https://doi.org/10.1002/grl.50115.

Fukumori, I., O. Wang, I. Fenty, G. Forget, P. Heimbach, and R. Ponte, 2020a: ECCO central estimate (version 4 release 4). ECCO Consortium, accessed 11 October 2020, https://www.ecco-group.org.

——, ——, ——, ——, ——, and ——, 2020b: Synopsis of the ECCO central production global ocean and sea-ice state estimate (version 4 release 4). ECCO Consortium, accessed 11 October 2020, https://doi.org/10.5281/zenodo.3765929.

Gill, A. E., 1982: *Atmosphere-Ocean Dynamics*. Academic Press, 682 pp.

Goni, G., M. Baringer, and F. Bringas, 2017: Florida Current transport in North Atlantic Ocean derived from satellite altimetry

observations (NCEI Accession 0157747). NOAA National Centers for Environmental Information, accessed 30 April 2020, https://doi.org/10.7289/v55b00ht.

Greatbatch, R. J., and A. Goulding, 1989: Seasonal variations in a linear barotropic model of the North Atlantic driven by the Hellerman and Rosenstein wind stress field. *J. Phys. Oceanogr.*, **19**, 572–595, https://doi.org/10.1175/1520-0485(1989)019<0572:SVIALB>2.0.CO;2.

Hameed, S., 2020: Atmospheric centers of action indices. Stony Brook University, https://you.stonybrook.edu/coaindices.

——, and S. Piontkovski, 2004: The dominant influence of the Icelandic Low on the position of the Gulf Stream northwall. *Geophys. Res. Lett.*, **31**, L09303, https://doi.org/10.1029/2004GL019561.

Hurrell, J. W., 1995: Decadal trends in the North Atlantic Oscillation: Regional temperatures and precipitation. *Science*, **269**, 676–679, https://doi.org/10.1126/science.269.5224.676.

——, Y. Kushnir, G. Ottersen, and M. Visbeck, 2003: An overview of the North Atlantic Oscillation. *The North Atlantic Oscillation: Climatic Significance and Environmental Impact*, *Geophys. Monogr.*, Vol. 134, Amer. Geophys. Union, 1–35.

Jones, D. C., G. Forget, B. Sinha, S. A. Josey, E. J. D. Boland, A. J. S. Meijers, and E. Shuckburgh, 2018: Local and remote influences on the heat content of the Labrador Sea: An adjoint sensitivity study. *J. Geophys. Res. Oceans*, **123**, 2646–2667, https://doi.org/10.1002/2018JC013774.

Joyce, T. M., C. Deser, and M. A. Spall, 2000: The relation between decadal variability of subtropical mode water and the North Atlantic Oscillation. *J. Climate*, **13**, 2550–2569, https://doi.org/10.1175/1520-0442(2000)013<2550:TRBDVO>2.0.CO;2.

Kalnay, E., and Coauthors, 1996: The NCEP/NCAR reanalysis 40-year project. *Bull. Amer. Meteor. Soc.*, **77**, 437–471, https://doi.org/10.1175/1520-0477(1996)077<0437:TNYRP>2.0.CO;2.

Kostov, Y., and Coauthors, 2021: Distinct sources of interannual subtropical and subpolar Atlantic overturning variability. *Nat. Geosci.*, **14**, 491–495, https://doi.org/10.1038/s41561-021-00759-4.

Larsen, J. C., and F. T. Smith, 1992: Transport and heat flux of the Florida Current at 27°N derived from cross-stream voltages and profiling data. *Philos. Trans. Roy. Soc. London*, **A338**, 169–236, https://doi.org/10.1098/rsta.1992.0007.

Lin, Y., R. J. Greatbatch, and J. Sheng, 2009: A model study of the vertically integrated transport variability through the Yucatan Channel: Role of Loop Current evolution and flow compensation around Cuba. *J. Geophys. Res.*, **114**, C08003, https://doi.org/10.1029/2008JC005199.

Marshall, J., A. Adcroft, C. Hill, L. Perelman, and C. Heisey, 1997: A finite-volume, incompressible Navier Stokes model for studies of the ocean on parallel computers. *J. Geophys. Res.*, **102**, 5753–5766, https://doi.org/10.1029/96JC02775.

——, H. Johnson, and J. Goodman, 2001: A study of the interaction of the North Atlantic oscillation with ocean circulation. *J. Climate*, **14**, 1399–1421, https://doi.org/10.1175/1520-0442(2001)014<1399:ASOTIO>2.0.CO;2.

McCarthy, G. D., and Coauthors, 2015: Measuring the Atlantic meridional overturning circulation at 26°N. *Prog. Oceanogr.*, **130**, 91–111, https://doi.org/10.1016/j.pocean.2014.10.006.

Meinen, C. S., M. O. Baringer, and R. F. Garcia, 2010: Florida Current transport variability: An analysis of annual and longer-period signals. *Deep-Sea Res.*, **57**, 835–846, https://doi.org/10.1016/j.dsr.2010.04.001.

Mildner, T. C., C. Eden, and L. Czeschel, 2013: Revisiting the relationship between Loop Current rings and Florida Current transport variability. *J. Geophys. Res. Oceans*, **118**, 6648–6657, https://doi.org/10.1002/2013JC009109.

Osychny, V., and P. Cornillon, 2004: Properties of Rossby waves in the North Atlantic estimated from satellite data. *J. Phys. Oceanogr.*, **34**, 61–76, https://doi.org/10.1175/1520-0485(2004)034<0061:PORWIT>2.0.CO;2.

Pérez-Hernández, M. D., and T. M. Joyce, 2014: Two modes of Gulf Stream variability revealed in the last two decades of satellite altimeter data. *J. Phys. Oceanogr.*, **44**, 149–163, https://doi.org/10.1175/JPO-D-13-0136.1.

Piecuch, C. G., R. M. Ponte, C. M. Little, M. W. Buckley, and I. Fukumori, 2017: Mechanisms underlying recent decadal changes in subpolar North Atlantic Ocean heat content. *J. Geophys. Res. Oceans*, **122**, 7181–7197, https://doi.org/10.1002/2017JC012845.

Riemer, N., O. M. Doherty, and S. Hameed, 2006: On the variability of African dust transport across the Atlantic. *Geophys. Res. Lett.*, **33**, L13814, https://doi.org/10.1029/2006GL026163.

Rossby, C.-G., 1939: Relation between variations in the intensity of the zonal circulation of the atmosphere and the displacement of the semi-permanent centers of actions. *J. Mar. Res.*, **2**, 38–55, https://doi.org/10.1357/002224039806649023.

Rossby, T., and R. L. Benway, 2000: Slow variations in the mean path of the Gulf Stream east of Cape Hatteras. *Geophys. Res. Lett.*, **27**, 117–120, https://doi.org/10.1029/1999GL002356.

Sanchez-Franks, A., S. Hameed, and R. E. Wilson, 2016: The Icelandic low as a predictor of the Gulf Stream north wall position. *J. Phys. Oceanogr.*, **46**, 817–826, https://doi.org/10.1175/JPO-D-14-0244.1.

Seager, R., R. Murtugudde, N. Naik, A. Clement, N. Gordon, and J. Miller, 2003: Air–sea interaction and the seasonal cycle of the subtropical anticyclones. *J. Climate*, **16**, 1948–1966, https://doi.org/10.1175/1520-0442(2003)016<1948:AIATSC>2.0.CO;2.

Serreze, M. C., F. Carse, R. G. Barry, and J. C. Rogers, 1997: Icelandic low cyclone activity: Climatological features, linkages with the NAO, and relationships with recent changes in the Northern Hemisphere circulation. *J. Climate*, **10**, 453–464, https://doi.org/10.1175/1520-0442(1997)010<0453:ILCACF>2.0.CO;2.

Taylor, A. H., and J. A. Stephens, 1998: The North Atlantic Oscillation and the latitude of the Gulf Stream. *Tellus*, **50A**, 134–142, https://doi.org/10.3402/tellusa.v50i1.14517.

Volkov, D. L., R. Domingues, C. S. Meinen, R. F. Garcia, M. Baringer, G. Goni, and R. H. Smith, 2020: Inferring Florida Current volume transport from satellite altimetry. *J. Geophys. Res. Oceans*, **125**, e2020JC016763, https://doi.org/10.1029/2020JC016763.

Wolfe, C. L. P., S. Hameed, and L. Chi, 2019: On the drivers of decadal variability of the Gulf Stream north wall. *J. Climate*, **32**, 1235–1249, https://doi.org/10.1175/JCLI-D-18-0212.1.